CORA Cork Open Research Archive
Cartlann Taighde Oscailte Chorcaí

Title	The high frequency electrical properties of interconnects on a flexible polyimide substrate including the effects of humidity
Author(s)	McGibney, Eoin; Barton, John; Floyd, Liam; Tassie, Paul; Barrett, John
Publication date	2011-01
Original citation	McGibney, E.; Barton, J.; Floyd, L.; Tassie, P.; Barrett, J (2011) 'The High Frequency Electrical Properties of Interconnects on a Flexible Polyimide Substrate Including the Effects of Humidity'. IEEE Transactions on Components, Packaging and Manufacturing Technology, 1 (1):4-15. doi: 10.1109/TCPMT.2010.2100731
Type of publication	Article (peer-reviewed)
Link to publisher's version	http://ieeexplore.ieee.org/stamp/stamp.jsp?tp=&arnumber=5734805&isnumber=5738414 http://dx.doi.org/10.1109/TCPMT.2010.2100731 Access to the full text of the published version may require a subscription.
Rights	**© 2011 IEEE. Personal use of this material is permitted. Permission from IEEE must be obtained for all other uses, in any current or future media, including reprinting/republishing this material for advertising or promotional purposes, creating new collective works, for resale or redistribution to servers or lists, or reuse of any copyrighted component of this work in other works.**
Item downloaded from	http://hdl.handle.net/10468/422

Downloaded on 2017-02-12T08:29:09Z

UCC
University College Cork, Ireland
Coláiste na hOllscoile Corcaigh

McGibney, E.; Barton, J.; Floyd, L.; Tassie, P.; Barrett, J.; , "The High Frequency Electrical Properties of Interconnects on a Flexible Polyimide Substrate Including the Effects of Humidity," *Components, Packaging and Manufacturing Technology, IEEE Transactions on* , vol.1, no.1, pp.4-15, Jan. 2011
doi: 10.1109/TCPMT.2010.2100731
http://ieeexplore.ieee.org/stamp/stamp.jsp?tp=&arnumber=5734805&isnumber=5738414

© 2011 IEEE. Personal use of this material is permitted. Permission from IEEE must be obtained for all other uses, in any current or future media, including reprinting/republishing this material for advertising or promotional purposes, creating new collective works, for resale or redistribution to servers or lists, or reuse of any copyrighted component of this work in other works.

CORA Cork Open Research Archive http://cora.ucc.ie

The High Frequency Electrical Properties of Interconnects on a Flexible Polyimide Substrate Including the Effects of Humidity

Eoin McGibney, John Barrett, John Barton, Liam Floyd, and Paul Tassie

Abstract—**Flexible circuit board materials can be used to advantage in radio frequency and high-speed digital systems but an obstacle to their use is the lack of availability of information on the electrical properties of materials to high frequencies and, in particular, the variation in dielectric constant and loss tangent as a function of frequency. This makes accurate electromagnetic simulation of high frequency flexible interconnects difficult. The variation of the electrical properties of these materials as a function of environmental parameters, such as humidity, is also unknown at higher frequencies. This paper has, using microwave resonators, investigated the electrical properties from 2 GHz to 18 GHz of a polyimide flexible circuit board material saturated at 25% RH and at 85% RH relative humidity levels. Rigid circuit board materials FR4 and CER-10 were also measured as reference materials. The relative permittivity, ε_r, total loss, α_T, and loss tangent, tan δ, have been extracted from the measurements for each material. The strong influence of conductor losses on overall losses when using thin materials such as flex at high frequency has also been evaluated and quantified in these measurements. In addition to the resonators used for measurement of material electrical properties, microstrip transmission lines were also included on each test sample and their s-parameters were measured at the same time and under the same conditions as the resonators. Comparisons between the measured electrical performance of the microstrip transmission lines and simulations of the lines based on the extracted material parameters show a high degree of correlation, indicating the validity of both the use of the resonator approach and overall loss measurement methodologies.**

Index Terms—**Electrical characterization, flexible substrates, high frequency, material properties.**

I. Introduction

THE USE OF printed circuit boards (PCBs) for high frequency applications, either radio frequency (RF) or high-speed digital, requires a detailed description of the frequency-dependent dielectric properties, dielectric constant and loss tangent, and of conductor losses so that overall losses and dispersion can be modeled using an EM simulator. It is critical for simulation accuracy that the simulation input information includes the electrical characteristics of the interconnect material(s) across all of the application bandwidth [1] and, where relevant, the variation of these properties with ambient environmental parameters such as temperature and humidity. Having this information available can allow the use of lower cost conventional PCB dielectric materials even to high frequencies [2]. While new materials are constantly emerging for both packages and circuit boards, relatively little has been published on the effect of environmental parameters, particularly moisture, on the high frequency electrical properties of even long established interconnect materials. This problem is greater for newer materials. Moulding compounds, encapsulants, underfills and PCB dielectrics all strongly influence the high frequency electrical performance of interconnects but we lack information on electrical properties, particularly dielectric constant and loss tangent, over wide bandwidths as a function of moisture content. The reliability of electrical simulations for interconnects fabricated from these materials and subject to electrical property changes on absorbing moisture is therefore open to question. An example of this is to be found in [3], where a flexible antenna for outdoor use showed significant change in electrical properties on absorption of moisture. There is also a growing use, for cost saving, of materials that were not necessarily originally intended for use at higher frequencies. Flexible substrates such as polyimide are being commonly used to increase system level integration in laptop computers, mobile phones, and connector systems and they are seeing growing use in RF applications for the purposes of increasing component density, miniaturization and conforming to awkwardly shaped spaces [4], [5]. The mechanical characteristics of flexible substrates make them attractive for these applications but very little information has been published describing their overall high frequency electrical characteristics, including both conductor and dielectric performance, or the effect of dielectric moisture absorption on microstrip configurations.

Therefore, the work described in this paper was undertaken to:

1) identify appropriate test structures and procedures for measurement of the high frequency electrical properties

Manuscript received April 1, 2009; revised March 8, 2010; accepted April 5, 2010. This work was supported by the SFI-Funded National Access Program (NAP-72), and by PRTL Strand 3 under the M-Zones Project. Recommended for publication by Associate Editor J. J. Liu upon evaluation of reviewers' comments.

E. McGibney is with the Digital Video Product Group, Analog Devices, Limerick, Ireland (e-mail: eoin.mcgibney@analog.com).

AQ:1 J. Barrett is with the Cork Institute of Technology (CIT), Bishopstown, Cork, Ireland (e-mail: john.barrett@cit.ie).

J. Barton is with the Tyndall National Institute, Cork, Ireland (e-mail: john.barton@tyndall.ie).

Color versions of one or more of the figures in this paper are available online at http://ieeexplore.ieee.org.

Digital Object Identifier 10.1109/TCAPT.2010.2055158

1521-3331/$26.00 © 2010 IEEE

IEEE Proof

of copper interconnects on a flexible PCB dielectric and the dielectric properties for the flex material;

2) extract conductor losses, dielectric constant, and loss tangent data up to 18 GHz from the measured s-parameter data;
3) examine the variation in the dielectric properties of materials after absorption of moisture;
4) compare the electrical properties of the flexible material with those of two common rigid PCB dielectrics;
5) verify the measurement and extraction methodologies by comparing measured and EM model results of microstrip validation structures.

The results in this paper present the characterization of copper interconnects fabricated on a flexible PCB over a 2 GHz to 18 GHz bandwidth; the separation of the different contributions of conductor and dielectric losses to overall losses as a function of frequency and moisture absorption; and cross-verification using microstrip interconnects representative of the "as manufactured" interconnects that would be used on a high-frequency PCB. Additionally, practical issues such as high frequency probing and measurement on double sided flexible substrates using via-less launches are discussed.

II. Related Work

The emphasis in this paper is on "overall" loss characterization, including conductor and dielectric losses, as it is this overall loss that is most relevant to design of real interconnects. The selection of test structures therefore focused on structures that could be used for extraction of total losses. Resonators are frequently applied for the study of microstrip dispersion and material properties [6], [7] and are suitable for the measurement of microstrip quality factor (Q-factor) or total loss. Examples of recent research published in this field [7]–[9] demonstrate the application of resonator approaches for the determination of relative permittivity and loss tangent of rigid PCB materials. In these studies, ring resonator, T-junction ($\lambda/4$ wave), and line resonator structures were used to determine the material properties of FR4, BT, and liquid crystal polymer (LCP) substrates. In addition to the study of the high frequency characteristics of materials, the change in material properties with temperature for an FR4 type substrate has also been reported in [9]. This paper [9] evaluated the change in both material properties with both humidity and temperature. When using resonators for dielectric characterization, conductor loss is usually a discarded by-product of the extraction of dielectric properties from overall loss measurements; in this paper they are retained to present a complete picture of overall interconnect losses and of the relative impact of each component of loss on overall loss.

III. General Approach

The electrical quantities to be experimentally measured and modeled over the measured frequency band are conductor loss, relative permittivity, ε_r and the loss tangent, tan δ. A two-port microstrip resonator approach was implemented to characterize the flexible substrate. The results of a two-port s-parameter measurement of each resonator structure facilitated the extraction of the three desired electrical properties. The relative permittivity was determined by the relationship between the physical length of the resonator and the measured resonant frequency, f_{res}. Subtracting conductor loss, α_C, from the measured total loss, α_T, determined dielectric loss and allowed calculation of the loss tangent. The flexible substrate material characterized was Sheldahl NovaClad [10]. Two rigid PCB dielectrics, FR4 (a very widely used low to moderate frequency substrate) and Taconic CER-10 [11] (a commonly used high frequency composite substrate), were also included in the tests both for comparison purposes and also to verify the general applicability of the measurement and extraction methodologies. All substrates were double-sided PCBs, consisting of a copper ground plane and a single signal layer. These materials were characterized using the same resonator methods as the flexible substrate.

While dielectric constant can be isolated from the measured resonator resonant frequency, f_{res}, relatively straightforwardly, the calculation of dielectric loss from total resonator loss measurement requires the separation of both conductor and radiation losses from the total loss. This approach relies on the use of empirical equations to approximate these losses. The calculation of both losses using these equations is sensitive to uncertainties in fabricated geometry, in particular substrate height, conductor thickness, and surface roughness. Knowledge of the post-fabrication resonator physical length is also required to accurately determine the effective permittivity, ε_{eff}, from the measured f_{res}. Post test sample fabrication metrology of x, y, and z-dimensions was therefore performed to identify deviations from design dimensions. These measurements also included measurement of conductor surface roughness. The expressions used for the calculation of the conductor and radiation loss were chosen from the literature [12]–[14], were implemented using C-code and used to automatically generate a file describing all loss and dispersion parameters across the measured frequency range for each of the samples. Extensive empirical studies [15]–[17] have published expressions for the prediction of the effective dielectric permittivity of substrates and of microstrip dispersion. These equations have previously been evaluated by York in [18] and, based on these findings, the equations presented by Kobayshi [15] were used in this paper. A comparison between empirical equations and measured results is included in Section VII.

A. Extraction of $\varepsilon_r(f)$ from $\varepsilon_{\text{eff}}(f)$

The resonant frequencies of the resonators were estimated during the design phase using the equations given in [17]. The measured resonant frequency and the resonator length of the fabricated resonators were used to calculate the effective relative permittivity, ε_{eff}(f), of the substrate materials across the measurement bandwidth. The relative permittivity of each substrate material was calculated using (1)–(3) as presented in [7]. These equations use the geometry of the substrate and observed ε_{eff}(f) to calculate ε_r(f)

$$\varepsilon_r(f) = \frac{2\varepsilon_{eff}(f) + M - 1}{M + 1} \quad (1)$$

IEEE Proof

$$M = \left(\frac{1+12h}{w_{eff}}\right)^2 \quad (2)$$

$$w_{eff} = w + (1.25t/\pi)\left[1+\ln(2h/t)\right] \quad (3)$$

where h is the substrate height, w is the microstrip line width, w_{eff} is the calculated effective microstrip width, and t is the microstrip line thickness.

B. Extraction of Dielectric Loss

The total loss (α_T) was determined from the measured Q-factor of each resonator. The total loss has three components: the conductor loss (α_c), the dielectric loss (α_d), and radiation losses (α_r). Applying (4)–(6) to the measured data yielded the total loss. Empirical expressions [12]–[14], [19] were used to approximate the conductor and radiated loss of the microstrip line on each substrate

$$\alpha_T = \alpha_c + \alpha_d + \alpha_r$$
$$\alpha_T(Np/m) = \frac{\pi}{Q_O \lambda_g} \quad (4)$$

$$Q_L = \frac{f_{res}}{BW_{-3\,dB}}$$
$$Q_O = \frac{Q_L}{1-10^{(-IL/20)}} \quad (5)$$

where Q_L and Q_o are the loaded and unloaded Q-factors, IL is the measured insertion loss at resonance, $\mathrm{BW}_{-3\,dB}$ is the -3 dB bandwidth of the resonant peak and λ_g is the guide wavelength.

Isolating the dielectric loss from the measured total loss allowed tanδ, the loss tangent, to be calculated, tan δ is extracted from the dielectric loss by [7]

$$\tan\delta = \frac{\alpha_d \lambda_0}{27.3} \cdot \frac{(\varepsilon_r - 1)\sqrt{\varepsilon_{eff}}}{\varepsilon_r(\varepsilon_{eff} - 1)}. \quad (6)$$

C. Environmental Effects Setup

To evaluate the influence of moisture absorption on the electrical properties of each substrate the experimental measurements were repeated after the materials have been exposed to moisture. Previous research in the area of moisture diffusion in PCB substrate materials was used to select the moisture soak conditions [20]. Moisture absorption in polymer materials generally obeys Fick's law, thereby defining the relationship between the moisture absorption ratio, M, exposure time, t, and thickness of the material, d, as the relationship given by

$$M \propto \frac{\sqrt{t}}{d}. \quad (7)$$

Data presented in [20] shows that a polyimide film of thickness 125 μm begins to saturate after moisture ratio of greater than 200 (625 min) is reached. Therefore, Sheldahl samples (thickness of $\sim 50\,\mu$m) were exposed to 85/85 relative humidity conditions for a period of 24 h (1440 min). It was envisaged that this period would ensure that the material would be sufficiently saturated. A saturated condition was preferred as it is the worst-case scenario for the effect of humidity on the flexible substrate. Both rigid dielectrics were exposed to the same relative humidity conditions but for a 48 h period.

TABLE I

DESIGN PARAMETERS FOR EACH SUBSTRATE, RELATIVE PERMITTIVITY, AND LOSS TANGENT FIGURES ARE TYPICAL VALUES FROM MANUFACTURERS' DATASHEETS

Substrate	ε_r	tan δ	Substrate Thickness	Line Width) (Zo≈ 50 Ω)	Cu Thickness
Sheldahl	3.3	0.011	48 μm	100 μm	10.2 μm
Taconic CER10	9.5 ± 0.5	0.0035	583.51 μm	0.635 mm	48.8 μm
FR4	4.4	0.0017	1491.75 μm	1.6 mm	35 μm

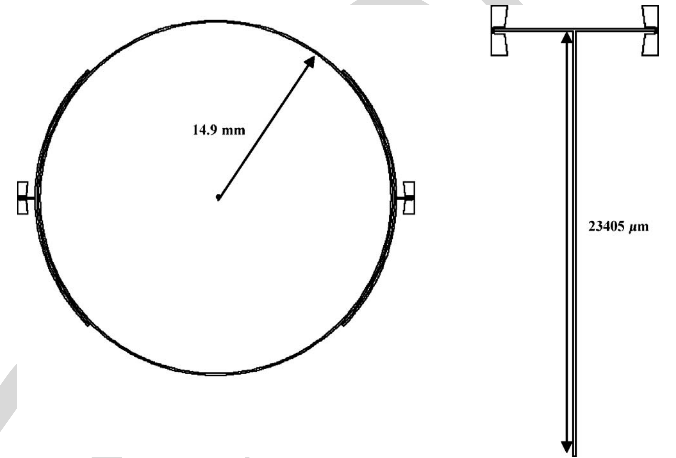

Fig. 1. 2 GHz microstrip ring resonator and quarter wave resonators on Sheldahl substrate.

IV. RESONATOR STRUCTURES

Microstrip ring and quarter-wave PCB resonator structures were designed and fabricated on each of the test substrates. The principal parameter relevant in determining the fundamental resonant frequency, f_0, of the resonator is the physical length, l_{res}; in the case of the ring resonator it is the mean radius, r_m. By varying l_{res} and r_m, the f_0 of each individual resonator was chosen at various frequency points from 1 GHz–12 GHz. Multiples of these frequencies also resonate at nf_0 where $n = 1, 2, 3, ..$, thereby covering the 2 GHz–20 GHz measurement frequency range. The physical material specifications and design parameters of each substrate material are summarized in Table I. These parameters are manufacturers' typical specifications and results of the post fabrication dimensional measurements. These parameters were used to calculate the static characteristic impedance, static effective permittivity $\varepsilon_{\mathrm{eff}}(0)$, and guide wavelength λ_g.

An example of each resonant structure is given in Fig. 1; in each case the annotated dimensions are the calculated values for a 2 GHz resonator structure fabricated on the Sheldahl substrate. Where used, edge-coupling gaps were chosen to lightly couple energy to each resonator and the gaps are typically twice the line widths. Coupling gaps of this width result in an S_{21} of approximately -30 dB to -40 dB at resonance. This level of coupled energy ensured the resonators did not become loaded during measurements.

Relating the physical length of each resonator to the electrical wavelength, the physical dimensions for each structure at a

particular resonant frequency can be determined (more detailed design procedures than can be presented here are available in [6], [17], and [21]). Equations (8)–(10) were used and the effective permittivity was calculated using the Kobayshi approximations

$$\lambda_g = \frac{c}{f\sqrt{\varepsilon_{eff}}} \tag{8}$$

$$l_{res} = n\lambda_g \tag{9}$$

$$r_m = \frac{n\lambda g}{2\pi} \tag{10}$$

where c is the speed of light in a vacuum = 2.99×10^8 m/s.

V. CPW Launches

Measurements on FR4 and CER10 substrates, being rigid, can be carried out using edge mount SMA connectors; due to the thinness (~50 μm) of the flexible substrate, this approach was not feasible without special fixturing. Therefore, high frequency coplanar (CPW) probes were used for the measurement of each of the substrates. The Gnd-Signal-Gnd configuration of the CPW probes required the design of a coplanar-to-microstrip transition. Typically, this is achieved through placement of adjacent ground pads either side of the signal line with plated via holes to a ground plane underneath forming the ground connection to each launch ground pad [22]. However, vias could not be fabricated in the double-sided flexible material process used in this paper. To overcome this problem, via-less coplanar probe-to-microstrip transitions were incorporated in the resonator designs. To facilitate high frequency measurements, the CPW launches need to exhibit good wideband performance. From a literature search, two suitable launch structures were found [23], [24]. Each of these structures has demonstrated wideband measurement capability on wafer level structures and neither requires vias. The suggested design equations presented in [23] and [24], combined with EM simulation, were used to obtain the final dimensions of both launches. The radial stub launch illustrated in Fig. 2, previously reported by Williams [23], demonstrated wideband performance for the measuring of s-parameters of MMICs using coplanar probes. The radial stub provides low impedance between the ground plane of the substrate and the ground pad of the coplanar probe. The 180° radial pattern is required for wideband performance. The length of the outer stub radius, l, is approximated from

$$l \approx \lambda_0/(2\pi\sqrt{\varepsilon_r}). \tag{11}$$

The impedance of the stub is lowest when the stub radius equals l and this is considered as the optimum stub. Using (11) as an initial condition a full wave EM simulation was used to tune the physical dimensions of the stub to yield an impedance minimum at 10 GHz. This is approximately the center frequency of the measurement bandwidth.

A second via-less CPW-to-microstrip transition was also implemented, shown in Fig. 3; this transition was designed using recommendations outlined by Zheng [24]. This transition is more compact than the radial stub and is more easily fabricated. The transition is composed of a CPW section for placement of the measurement probes and a transition section where the CPW mode is transformed to a quasi-static TEM mode propagating on a microstrip line. This is physically done using a controlled taper between the signal lines and adjacent ground planes. On the flexible substrate, only a slight taper was required as the designed microstrip line width (~100 μm) was comparable to the coplanar signal line width. For the measurements on the rigid boards more conventional CPW to microstrip launches were used. The design of the CPW launches for the rigid boards followed the layout guidelines recommended by [22]. A photograph of all of the resonant structures fabricated on the flexible substrate is shown in Fig. 4.

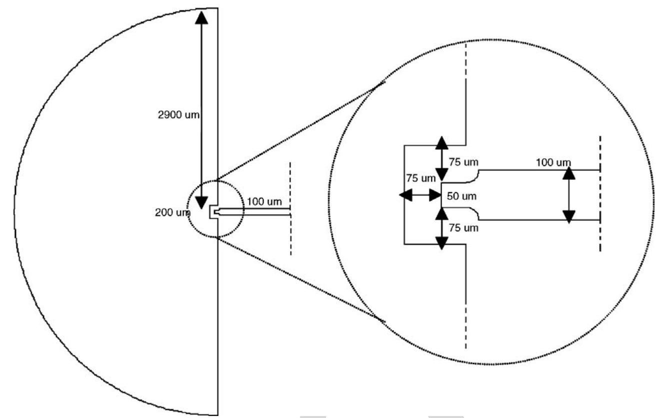

Fig. 2. Radial stub coplanar to microstrip launch.

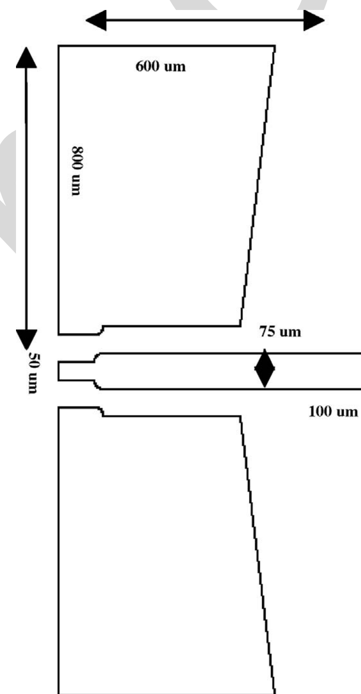

Fig. 3. Coplanar to microstrip transition.

VI. Measurements

S-parameter measurements were performed using an Agilent 8720D vector network analyzer with a frequency sweep

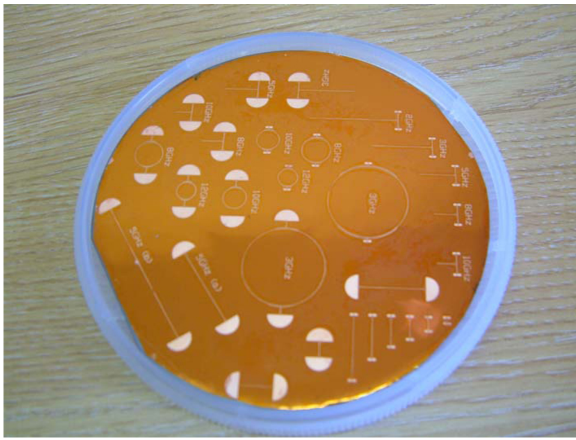

Fig. 4. Photograph of the fabricated structures on the flexible PCB (the flex-PCB is silicon wafer shaped because a former wafer mask aligner is used for photolithography).

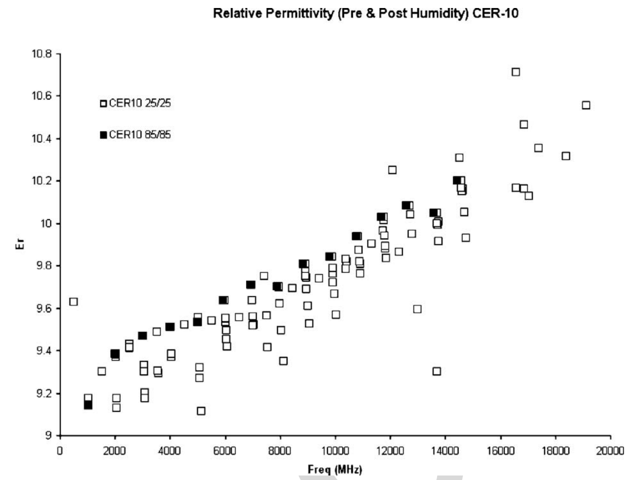

Fig. 6. Experimental determined relative permittivity of Taconic CER-10.

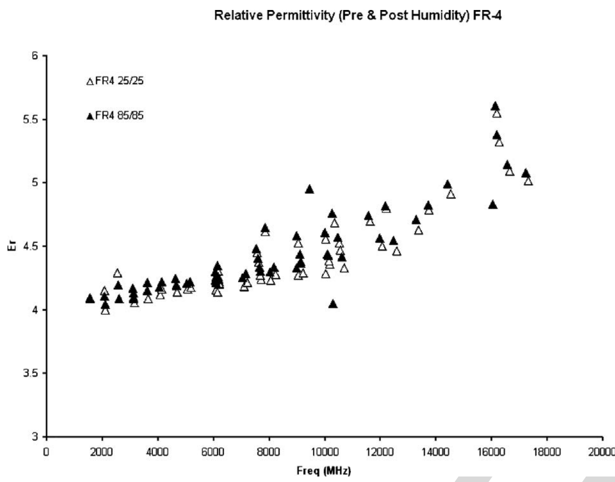

Fig. 5. Experimentally determined relative permittivity of FR4.

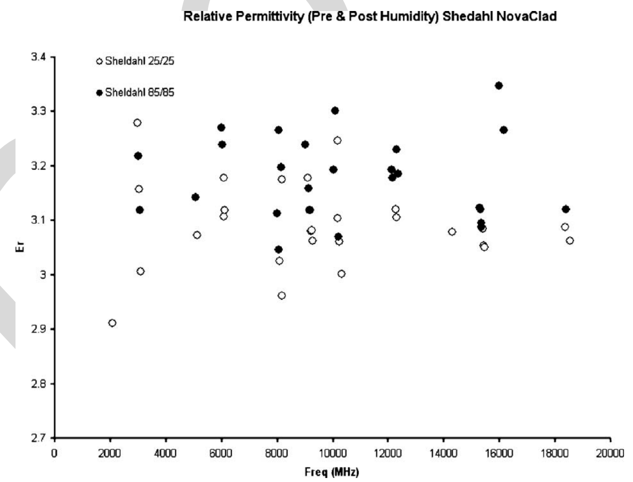

Fig. 7. Experimentally determined relative permittivity of Shedahl Nova-Clad.

from 50 MHz to 20 GHz and 801 sampling points, giving a raw frequency step size resolution of 24.904 MHz. All structures were measured using CPW probes with full two-port calibration applied to the ends of the probe tips using a TRL calibration method. The cascade Microtech impedance standard substrate was used to verify the calibration accuracy. Measurement files were captured for each individual structure and later post processed into Touchstone (.s2p) format and imported into an RF circuit simulator for analysis and parameter extraction.

VII. Results

A. Relative Permittivity

The measured s-parameters were imported into an RF circuit simulator as two-port s-parameter networks [25]. A frequency plot of the experimental s-parameter data for each structure was used to identify the resonant frequency, insertion loss and the −3 dB bandwidth at each resonant peak. The measured f_{res} and the measured fabricated resonator length were used to calculate the effective relative permittivity directly from the s-parameter measurements. The relative permittivity was extracted from this data using the method and equations previously outlined in Section III. A plot of the measured $\varepsilon_r(f)$ for the Sheldahl and control substrates is given in Figs. 5–7. The results plotted here include the results of both the ring and quarter wave resonators. In the frequency band of 3 GHz to 18 GHz the $\varepsilon_r(f)$ of the Sheldahl varies from 2.91 to 3.3 (7% increase) with a mean value of 3.15. This compares with the manufacturer's specification of 3.3 at 1 GHz. Additionally, the $\varepsilon_r(f)$ of the substrate remains relatively constant across the entire frequency band, a desirable characteristic for broadband design. In comparison to the control substrates there is greater variation in the Sheldahl results. This is attributable to manufacturing variations in the resonators since the difficulty of handling the flexible substrate in the laboratory level photo-patterning facilities used for this paper lead to a higher variability in resonator dimensions than for the rigid substrates. Aside from using commercial flex patterning, a facility which was not available for this paper, a possible solution would be to significantly increase the number of flex test samples (from the 14 used in this paper) and to use averaging to compensate for the manufacturing variations. For the Taconic

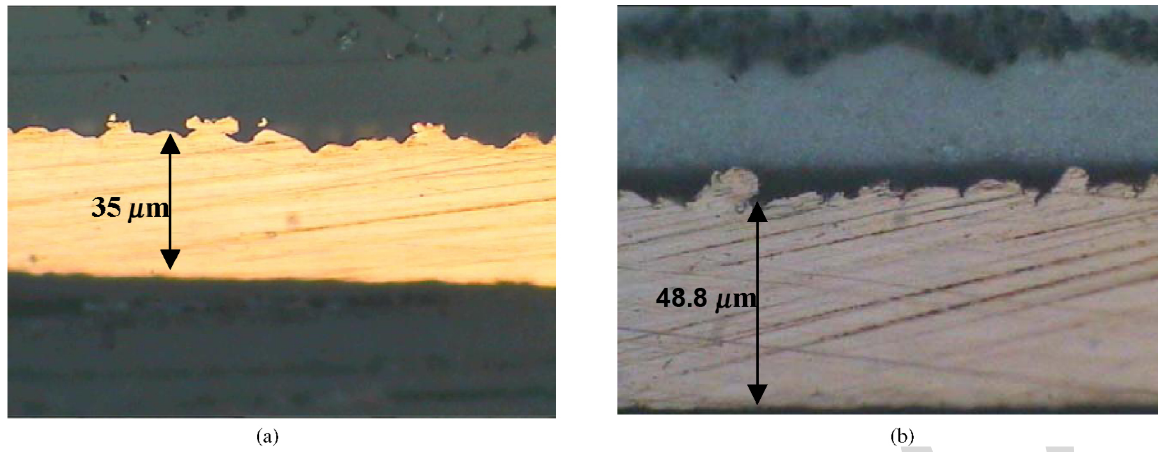

Fig. 8. Cross sections of the copper conductors fabricated on (a) FR4 and (b) CER10 at 500× magnification.

substrate the $\varepsilon_r(f)$ increases from 9.14 to 10.55 (15.43% increase) while the $\varepsilon_r(f)$ of the FR4 increases from 4.08 to 5.14 (25.9% increase) across the measurement bandwidth. A further observation is the comparison of results between resonators fabricated with the same resonant frequencies. In the case of the flexible substrate, the largest difference observed between resonators occurs at 10 GHz, where the difference in ε_r is ~8.3%. Therefore, either the ring or quarter wave resonant method yields the same results within an acceptable degree of measurement error. From a fabrication perspective, this is an important result as the quarter wave resonators are easier to fabricate and do not require the use of gap coupling to excite the resonator.

B. Conductor Loss

The conductor loss (α_c) for each microstrip structure was approximated using empirical equations reported by Collin [14]. These equations, which include loss due to surface roughness, have a reported accuracy of 6%–8%. Equations presented by Pucel [12], [13] were also evaluated but the predicted conductor loss for the microstrips on the flexible substrate was much higher and did not reflect the experimental results. The post fabrication dimensions, both magnified cross-sections and a profile measurement of the conductors were used to determine the surface roughness and improve the overall approximation of α_c. All conductors were fabricated of copper ($\sigma_{\text{ideal}} = 5.8 \times 10^7 \text{S/m}$) and no solder mask or finish was applied. Photographs of the cross section for the rigid substrates are shown in Figs. 8 and 9.

The average surface roughness for the copper on flex was ~1 μm, while it was ~5 μm for copper on the rigid substrates. The effect of this surface roughness was included in the calculation of conductor loss using a multiplication factor determined by [17]

$$\alpha_c = \alpha_c^{'} \left\{ 1 + \frac{2}{\pi} \tan^{-1} \left[1.4 \left(\frac{\Delta}{\delta_s} \right)^2 \right] \right\} \tag{12}$$

where δ_s is the skin depth, Δ is the measured surface roughness, and $\alpha_c^{'}$ is the calculated conductor attenuation without surface roughness included.

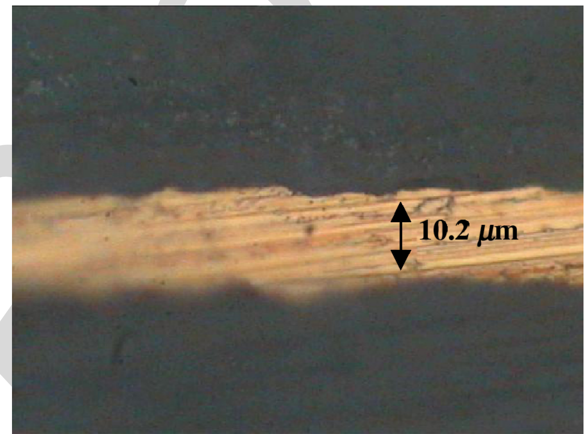

Fig. 9. Cross section of copper conductor on Sheldahl at 1000× magnification.

A plot of the calculated multiplication factors for specific levels of surface roughness is given in Fig. 10. A plot of the calculated conductor loss in dB/m for the microstrip structures on each substrate is shown in Fig. 11; from the plot it can be seen that the microstrip line on the flex exhibits the highest conductor loss per unit length. This is caused by the necessarily narrower line dimensions required to obtain any given line impedance on the thin flex when compared to the wider microstrip lines fabricated on the thicker control substrates.

C. Loss Tangent

Subtracting the calculated conductor and radiation loss from the measured total loss yields the loss attributable to the dielectric only. Radiation losses were determined for the open-ended quarter wave resonator using equations presented by Lewin [26] and Van der Pauw [19] but on all substrates it can be considered negligible (1.29 dB/m at 18 GHz on Sheldahl) when compared to conductor and dielectric losses.

The loss tangent is extracted from dielectric loss using (6), as previously outlined in Section II. The extracted loss tangent results for each test substrate are plotted across the measured frequency band in Figs. 12–14. The loss tangent of

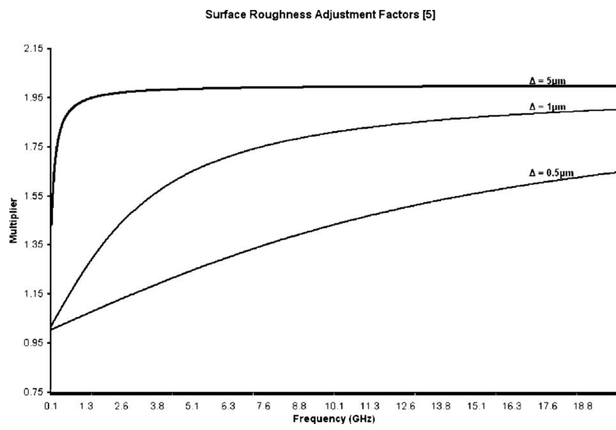

Fig. 10. Multiplier factor for the increase in conductor loss due to different surface roughness.

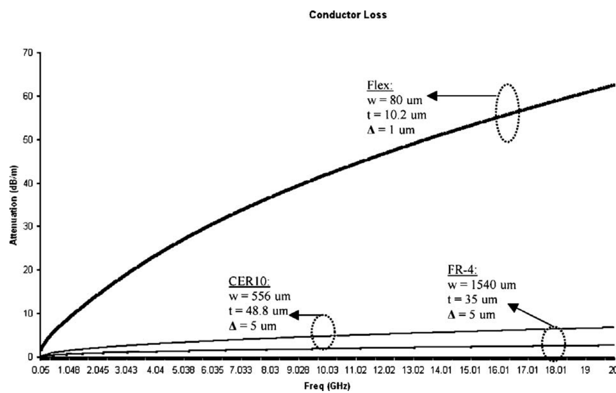

Fig. 11. Calculated conductor loss (dB/m) for each microstrip line using design equations presented by Collin [17].

the Sheldahl material ranges from 0.0078 at 3 GHz to 0.008 at 18 GHz and can be considered constant with frequency with an average value of 0.00683. This result is lower than the manufacturer specified value of 0.011. The difference between manufacturer specifications and the extracted values is attributed to the very high conductor loss relative to dielectric loss and the resultant increased difficulty in isolating the dielectric loss. Also included in the plot is the calculated loss tangent under 85/85 RH. Under these conditions the loss tangent increases to 0.0091 at 3 GHz but a decrease to 0.006 is seen at 18 GHz with an average value of 0.0077. The FR4 substrate has a measured loss tangent that ranges from 0.018 at 2.5 GHz to 0.044 at 16.5 GHz, these values compare well to results previously published by Heinola [9] for an FR4-type substrate. The results also show that the exposure to 85/85 RH conditions for a period of 48 h has no noticeable effect on the FR4 substrate. There are two reasons why the FR4 did not exhibit a large variation in material properties after exposure to the 85/85 RH conditions. The first is attributed to the short soak time applied to the FR4 samples, the second reason is the presence of the copper ground plane which acts as a barrier to moisture diffusion [27]. In previously published results for the material properties of FR4, the specified soak times at which FR4 reaches saturation are taken as 200–400 h [28] depending on glass/resin content. For the purposes of this experiment and in light of the previously published data

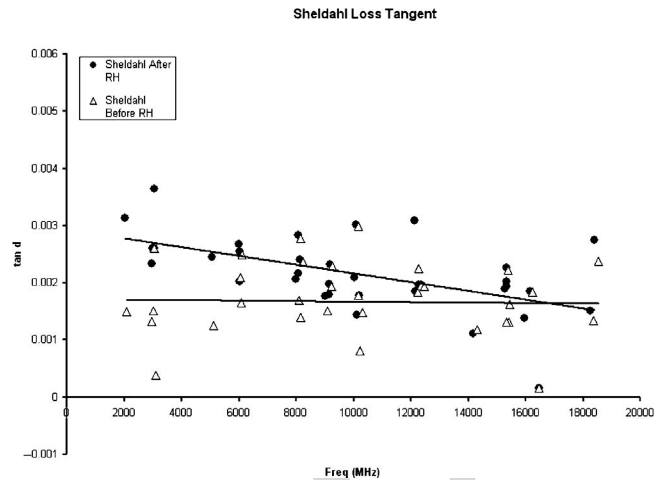

Fig. 12. Calculated loss tangent of Sheldahl substrate before and after RH exposure.

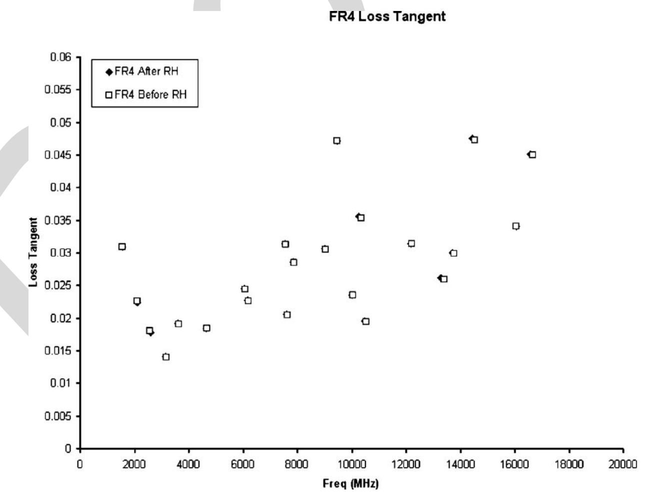

Fig. 13. Calculated loss tangent of FR-4 substrate before and after RH.

on FR4, the FR4 samples were only exposed to a soak time comparable with the soak time of the flexible substrate. A similar approach was taken with the CER10 samples. The manufacturer's datasheet for the CER10 substrate specifies excellent resistance to moisture absorption and this is verified by the experimental results.

The CER10 exhibits the lowest loss tangent values, ranging from 0.0034 at 2 GHz to 0.0047 at 18 GHz. As expected, this is an order of magnitude smaller than the other two substrates. After exposure to 85/85 RH conditions the variation in calculated loss tangent is within measurement variation. Therefore the differences in pre-humidity and post-humidity are attributed to noise in the s-parameter measurements and not due to moisture absorption.

D. Analysis of Flexible Substrate After RH Exposure

A precision weighing scales was used to determine the mass of the Sheldahl sample pre and post RH exposure. The mass of the sample pre RH exposure was measured as 1.03195 g, the post RH sample was measured as 1.03490 g. There was an increase of 2.95 mg in mass due to water absorption, giving a

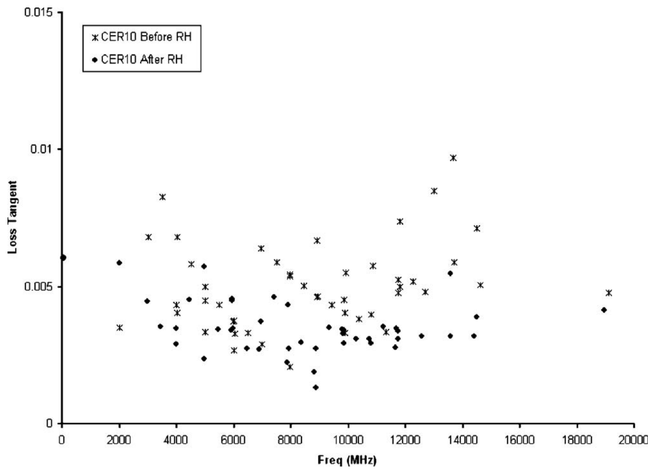

Fig. 14. Calculated loss tangent of CER-10 substrate before and after RH.

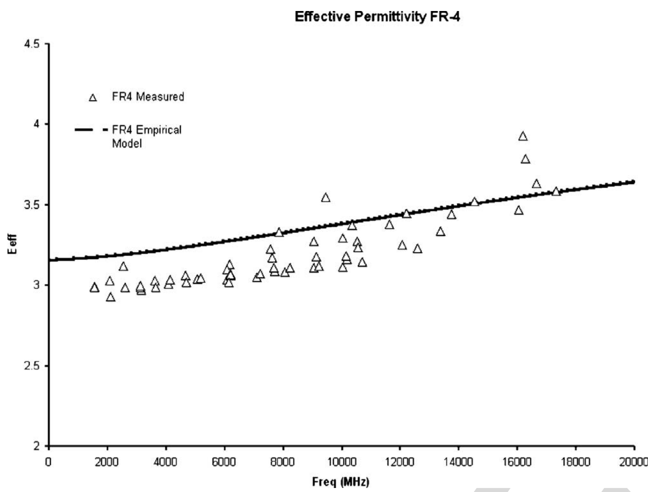

Fig. 15. Comparison of measured effective permittivity for FR4 to Kobayshi empirical equations [15].

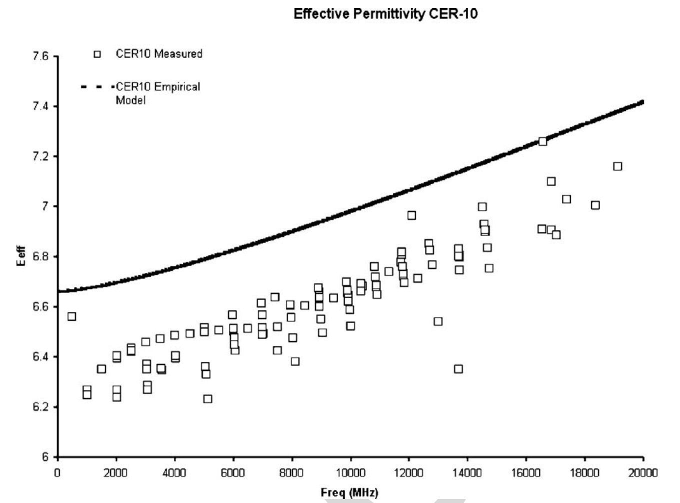

Fig. 16. Comparison of measured effective permittivity for CER10 to Kobayshi empirical equations [15].

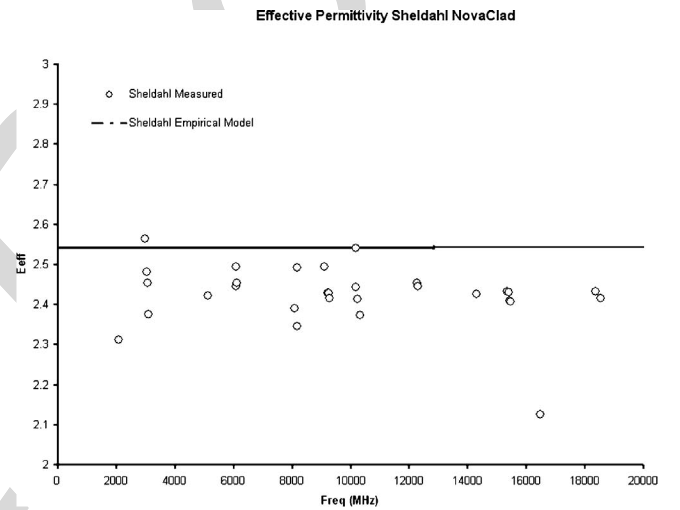

Fig. 17. Comparison of measured effective permittivity for Sheldahl Nova-Clad to Kobayshi empirical equations [15].

percentage moisture absorption ratio of 0.285%. At saturation, a polyimide sample typically has a moisture absorption ratio of 2% and the reduced moisture absorption here is attributed to the presence of a copper ground plane, which inhibits moisture diffusion. This reduced level of moisture absorption has been previously observed in organic laminate materials that have copper ground planes [27]. An increase in moisture content of ~0.3% would lead to an increase in capacitance between planes of 2.5%; considering the impedance of a microstrip line, this would lead to a decrease in characteristic impedance. Due to the presence of moisture, the average value of the experimentally determined loss tangent of the Sheldahl substrate has increased by approximately ~13.3% (increased from 0.0068 to 0.0077). The relative permittivity has increased by 5–10% after 85/85RH conditions, this increase in permittivity would cause a reduction in the propagation delay along an interconnect and also effect the characteristic impedance of the interconnect. Although the observed degree of moisture absorption was relatively small, it is clear that the sensitivity of transmission line electrical parameters to changes in loss tangent and dielectric constant can result in large variations of those parameters.

E. Comparison of Empirical Equations for the Prediction of $\varepsilon_{\mathrm{eff}}$

A comparison of three of the reportedly [18] most accurate empirical equations for dielectric constant, Edwards [17], Kirchning [16], and Kobayshi [15] was also included in this paper. The static effective permittivity, $\varepsilon_{\mathrm{eff}}(0)$, was calculated using two methods: the first was to extrapolate the measured effective permittivity data to a zero frequency point; the second used further empirical equations with the manufacturers' specifications to calculate a static effective permittivity value. The best results were observed when using an extrapolated value for the $\varepsilon_{\mathrm{eff}}(0)$ and the Kobayshi equations. A comparison of the Kobayshi model calculated using an empirically derived static effective permittivity to the measured values is plotted in Figs. 15–17. The empirical model, calculated using an extrapolated value for the static effective permittivity shows better correlation to the measured effective permittivity for all substrates. This is shown in Fig. 18. Using this approach could allow the approximation of effective permittivity outside

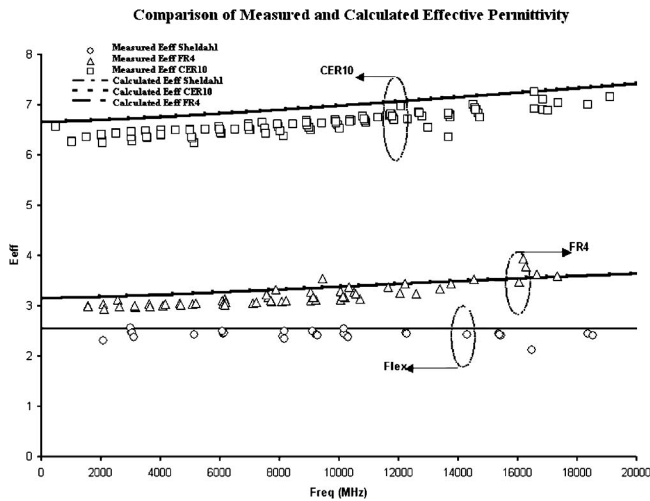

Fig. 18. Comparison of measured effective permittivity to Kobayshi empirical equation using a static effective permittivity extrapolated from measured data.

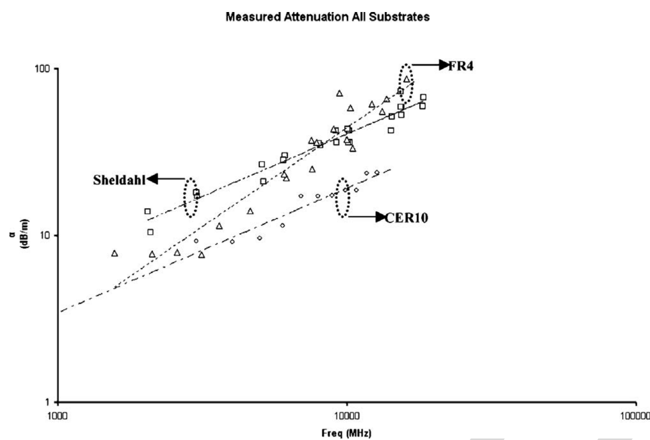

Fig. 19. Measured attenuation (dB/m) for each of the substrates.

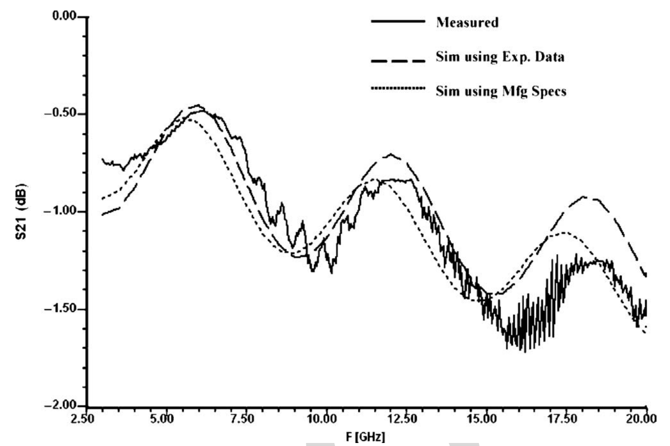

Fig. 20. Simulated and measured S21 (dB) for a 16 mm long microstrip line on flex.

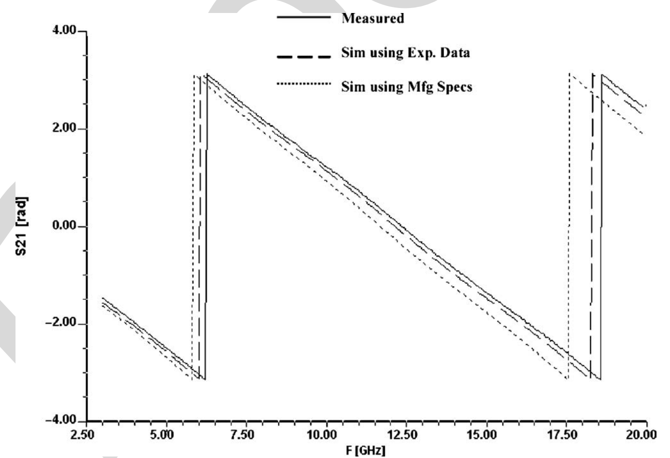

Fig. 21. Simulated and measured S21 (radians) for a 16 mm long microstrip line on flex.

the range of this paper. Although the calculations involved are relatively straightforward, it was noted that the equations presented by Edwards give a very good approximation and can easily be performed by hand.

F. Benchmarking Against Control Substrates

The loss tangent is one of the main metrics used to benchmark a high frequency substrate; the desirable qualities of a high frequency substrate are a consistent relative permittivity with frequency and a low loss tangent. Inspecting Figs. 12–14, the substrate with the lowest loss tangent is the Taconic CER-10 while both the FR4 and flexible substrate have comparable loss tangents. This analysis alone is not sufficient when comparing the high frequency performance of the substrates as the conductor loss that dominates the Sheldahl total loss must also be included. The measured total attenuation per meter for each substrate is plotted on a log-log scale in Fig. 19.

The use of a log-log scale is useful in determining the dominant loss mechanism [29], on this scale a slope of 0.5 is conductor loss while a slope equal to 1 characterizes dielectric losses. From the plot, both the Sheldahl and CER10 attenuation is dominated by conductor loss (slopes $\approx$ 0.7). In the case of the Sheldahl this is due to the narrow conductor, while for the CER10 this is due to the low dielectric loss compared to dielectric loss. The FR4 is dominated by dielectric loss (slopes $\approx$ 1). Therefore, it can be concluded that microstrip transmission lines with characteristic impedances in the region of $40\Omega - 60\Omega$ on a Sheldahl substrate of 48 μm will exhibit the highest loss up to 10 GHz. In comparison to the least lossy substrate (CER10) substrate, the flexible substrate exhibits twice the attenuation per unit length.

G. Validation

To evaluate the influence of using the measured data on simulation results, EM and RF circuit simulations of microstrip lines were performed. Microstrip lines of the same cross section but with varying lengths were fabricated with the resonator structure test coupons. S-parameter measurements were taken for each microstrip line over a 1 GHz to 20 GHz bandwidth. The geometry of the microstrip lines were used with the manufacturer's material specifications and the measured material properties to create microstrip models. One such model was generated and simulated using a commercial field solver (Sonnet EM [30]). The simulation was repeated twice, firstly using the average extracted frequency dependent

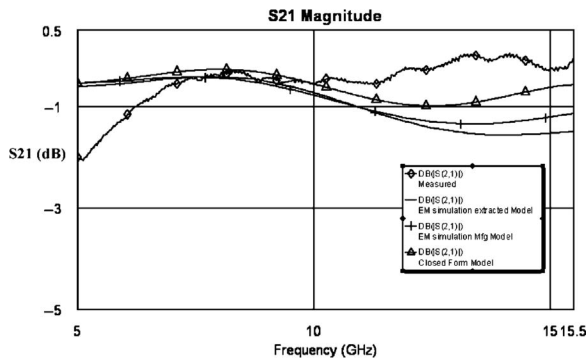

Fig. 22. S21 (dB) results from EM and circuit simulation of a 9.96 mm microstrip line on FR4 using manufacturer and measured material properties.

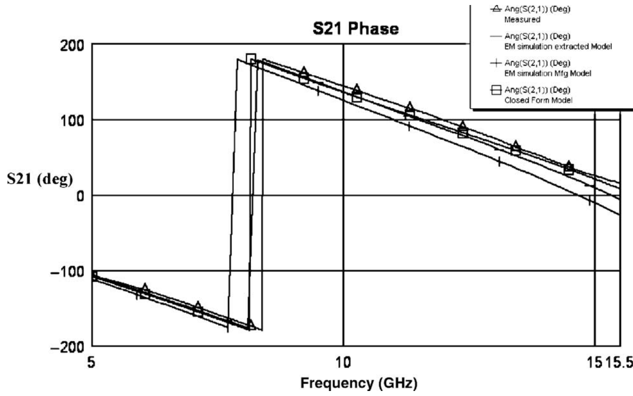

Fig. 23. S21 (deg) results from EM and circuit simulation of a 9.96 mm microstrip line on FR4 using manufacturer and measured material properties.

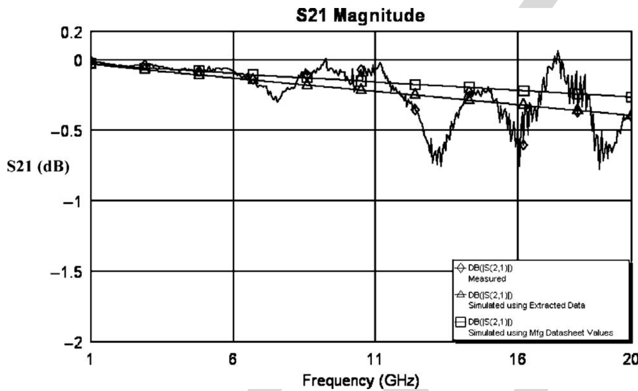

Fig. 24. S21 (dB) results from EM and circuit simulation of a 12 mm microstrip line on CER10 using manufacturer and measured material properties.

material (in the case of microstrip on Sheldahl: tan $\delta = 0.0068$ and $\varepsilon_r = 3.015$). To include the effects of conductor surface roughness the conductor conductivity that was adjusted. This "effective" conductivity, $\sigma_{\text{effective}}$, was calculated using an equation presented in [31] and given in

$$\sigma_{effective} = \left(\frac{\sigma_{ideal}}{(1 + e^{-(\delta/\Delta)^{1.6}})^2} \right) \tag{13}$$

where δ is the skin depth in μm and Δ is the surface roughness in μm.

The second simulation set-up used the static properties specified by the manufacturer datasheets (tan $\delta = 0.011$ and $\varepsilon_r = 3.3$) and ideal conductor properties. The s-parameter results of the simulations were compared in order to highlight the correlation between the predicted and measured s-parameters. In particular, a comparison was made between the magnitude and phase of the S21 parameter. This parameter was chosen as the both the loss (effected by tan δ and conductor conductivity) and propagation delay (effected by relative permittivity) is captured by this parameter. Figs. 20 and 21 plot the simulated and measured S21 results for a 16.07 mm long microstrip line with a line width of 59.67 μm fabricated on the Sheldahl substrate. By inspection of the plots it is seen that using the experimentally determined value for the relative permittivity gives a better prediction of the phase than using the manufacturer's value. In the case of the magnitude of S21, the experimentally determined loss tangent also gives a better prediction in the frequency range 4 GHz to 15 GHz. Outside of this range both simulation results begin to diverge from the measured result.

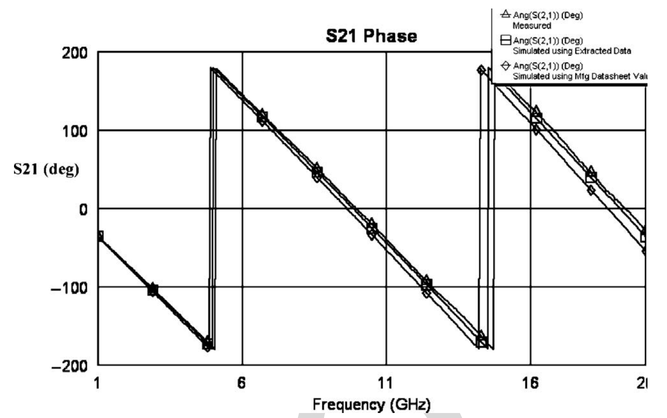

Fig. 25. S21 (deg) results from EM and circuit simulation of a 12 mm microstrip line on CER10 using manufacturer and measured material properties.

This type of simulation was also repeated for microstrip lines fabricated on both the FR4 and CER10 substrates. Average values for the substrate material properties were taken at the frequencies defined by manufacturers data. The results for the FR4 simulation of a 9.96 mm microstrip line are given in Figs. 22 and 23. Additionally, an RF circuit simulator was used to simulate a microstrip models that are defined by the manufacturers and measured material properties. The results of these simulations for a microstrip line fabricated on FR4 and CER10 are given in Figs. 22–25. As in the case of the EM simulation results the s-parameter response of the microstrip models defined by the measured material properties more closely match the measured results. From these results it can be seen that the measured relative permittivity and loss tangent values can be used to better model the actual as manufactured microstrip line than using manufacturer specifications.

VIII. Discussion and Conclusion

An investigation into the high frequency electrical properties of interconnects fabricated on a Sheldahl NovaClad substrate has been presented. The $\varepsilon_r(f)$, $\varepsilon_{\text{eff}}(f)$, tan$\delta$, conductor losses and total loss have been determined under ambient RH conditions and under 85/85 RH conditions. The flexible

595 substrate has an $\varepsilon_r(f)$ and $\tan\delta$, which varies from 2.91 to 596 3.119 and 0.0078 to 0.008 over the measured bandwidth. 597 There is variation in the extraction of the loss tangent values 598 from the measurements; this is attributed to the dependency 599 of the resonator approach on the estimation of conductor 600 losses. It has also been observed that the difference between 601 resonator methods is negligible in terms of determining the 602 relative permittivity. Since the quarter wave resonator does 603 not require coupling gaps and has dimensions that are easier 604 to control during fabrication this is the recommended approach 605 for determining the material properties of similar flexible 606 substrates. Additionally, it has been found that empirical equa-607 tions presented by Kobayshi give the best approximation of 608 the effective permittivity across the measured bandwidth. The 609 saturation of the flexible substrate did not obey Ficke's law due 610 to the presence of the copper ground plane, inhibiting moisture 611 diffusion. Therefore, the degree of moisture diffusion will 612 vary from application to application depending on the flexible 613 PCB stack up and metallization. Finally, the comparison of 614 the flexible substrate to the control substrates showed that 615 when used to as the carrier substrate for typical microstrip 616 line structures it would exhibit the largest loss per unit length 617 due to higher conductor losses. The validation of the extracted 618 material properties shows an improvement in the prediction of 619 the magnitude and phase of the s-parameters of a microstrip on 620 a flexible substrate and on the control substrates when using 621 experimentally extracted material properties and the concept 622 of an effective conductivity in place of the manufacturer's 623 datasheet values.

624 ACKNOWLEDGMENT

625 The authors would like to acknowledge the support of the 626 Tyndall National Institute, Cork, Ireland.

627 REFERENCES

628 [1] B. McDermott and S. McKinney, "Dielectric material properties: Es-629 sential inputs to an accurate signal-integrity analysis and high-reliability 630 design," in *Proc. DesignCon*, 2006. AQ:2

631 [2] D. Leys, "Best materials for 3–6 GHz design," *Printed Circuit Design 632 Manuf. Mag.*, pp. 34–39, Nov. 2004. AQ:3

633 [3] B. O'Flynn, J. Buckley, D. Laffey, J. Barton, and S. C. O'Mathuna, 634 "Simulation, design, development and test of antennas for wireless 635 sensor network systems," *Microelectron. Int.*, vol. 24, no. 2, pp. 3–6, 636 2007.

637 [4] M. S. Doyle, W. Martin, D. Pease, and T. Timpane, "Low-loss flex circuit 638 interconnect: Development of reduced insertion-loss flexible packaging," 639 in *Proc. 57th ECTC*, 2007, pp. 1870–1876.

640 [5] H. Braunisch, J. E. Jaussi, J. A. Mix, M. B. Trobough, B. D. Horine, 641 V. Prokofiev, L. Daoqiang, R. Baskaran, P. C. H. Meier, H. Dong-Ho, 642 K. E. Mallory, and M. W. Leddige, "High-speed flex-circuit chip-to-chip 643 interconnects," *IEEE Trans. Adv. Packag.*, vol. 31, no. 1, pp. 82–90, Feb. 644 2008.

645 [6] K. C. Chang, *Microstrip Ring Circuits and Related Structures*. New 646 York: Wiley, 2004.

647 [7] G. Zhou and H. Gronqvist, "Characterization of liquid crystal polymer 648 for high frequency system-in-a-package applications," *IEEE Trans. Adv. 649 Packag.*, vol. 25, no. 4, pp. 503–508, Nov. 2002.

650 [8] J. Heinola, "A method to evaluate effects of moisture absorption on 651 dielectric constant and dissipation factor of printed circuit board mate-652 rials," in *Proc. 9th Int. Symp. Adv. Packag. Mater. Processes, Properties 653 Interfaces*, 2004, pp. 241–246.

[9] K.-P. Latti, J.-M. Heinola, M. Kettunen, J.-P. Strom, and P. Silventoinen, 654 "A review of microstrip t-resonator method in determination of dielectric 655 properties of printed circuit board materials," in *Proc. IEEE IMTC*, May 656 2005, pp. 62–66. 657

[10] *Sheldahl NovaClad Technical Information* [Online]. Available: 658 http://www.sheldahl.com/Product/bulletins/g2300.pdf 659

[11] *CER10 Datasheet* [Online]. Available: http://www.taconic-660 add.com/pdf/cer10.pdf 661

[12] R. A. Pucel, D. J. Masse, and C. P. Hartwig, "Losses in microstrip," 662 *IEEE Trans. Microw. Theory Tech.*, vol. MTT-16, no. 6, pp. 342–350, 663 Jun. 1968. 664

[13] R. A. Pucel, D. J. Masse, and C. P. Hartwig, "Correction to losses in 665 microstrip (correspondence)," *IEEE Trans. Microw. Theory Tech.*, vol. 666 16, no. 12, p. 1064, Dec. 1968. 667

[14] R. E. Collin, *Foundations for Microwave Engineering*, 2nd ed. New 668 York: Wiley-IEEE, 2000. 669

[15] M. Kobayashi, "A dispersion formula satisfying recent requirements in 670 microstrip CAD," *IEEE Trans. Microw. Theory Tech.*, vol. 36, no. 8, pp. 671 1246–1250, Aug. 1988. 672

[16] M. Kirsching and R. H. Jansen, "Accurate model for effective dielectric 673 constant of microstrip with validity up to millimeter wave frequencies," 674 *Electron. Lett.*, vol. 18, no. 6, pp. 272–273, Mar. 1982. 675

[17] T. C. Edwards and M. B. Steer, *Foundations of Interconnect and 676 Microstrip Design*. Norwood, MA: Artech House, 2001. 677

[18] R. A. York and R. C. Compton, "Experimental evaluation of existing 678 CAD models for microstrip dispersion," *IEEE Trans. Microw. Theory 679 Tech.*, vol. 38, no. 3, pp. 327–328, Mar. 1990. 680

[19] L. J. van der Pauw, "The radiation of electromagnetic power by 681 microstrip configurations," *IEEE Trans. Microw. Theory Tech.*, vol. 25, 682 no. 9, pp. 719–725, Sep. 1977. 683

[20] Y. Shimamura, T. Urabe, A. Todoroki, and H. Kobayashi, "Measurement 684 of moisture absorption ratio of FRP using micro polymer sensor," *Key 685 Eng. Mater.*, vols. 270–273, pp. 1957–1964, Aug. 2004. 686

[21] J. Carroll, M. Li, and K. Chang, "New technique to measure transmission 687 line attenuation," *IEEE Trans. Microw. Theory Tech.*, vol. 43, no. 1, pp. 688 219–222, Jan. 1995. 689

[22] Layout rules for GHz probing. *Cascade MicroTech Application Note* 690 [Online]. Available: www.cmicro.com 691

[23] D. Williams and T. Miers, "A coplanar probe to microstrip transition," 692 *IEEE Trans. Microw. Theory Tech.*, vol. 36, no. 7, pp. 1219–1223, Jul. 693 1988. 694

[24] G. Zheng, J. Papapolymerou, and M. M. Tentzeris, "Wideband coplanar 695 waveguide RF probe pad to microstrip transitions without via-holes," 696 *IEEE Microw. Wirel. Compon. Lett.*, vol. 13, no. 12, pp. 544–546, Dec. 697 2003. 698

[25] Microwave Office [Online]. Available: http://web.awrcorp.com 699

[26] L. Lewin, "Spurious radiation from microstrip," *Proc. IEEE*, vol. 125, 700 no. 7, pp. 633–642, 1978. 701 AQ:4

[27] M. G. Pecht, H. Ardebili, A. A. Shukla, J. K. Hagge, and D. Jennings, 702 "Moisture ingress into organic laminates," *IEEE Trans. Compon. Packag. 703 Technol.*, vol. 22, no. 1, pp. 104–110, Mar. 1999. 704

[28] S. Khan, "Comparison of the dielectric constant and dissipation factors 705 of non-woven aramid/FR4 and Glass/FR4 laminates," Dupont Advanced 706 Fibers Systems Division, *Tech. Note*. 707 AQ:5

[29] A. Byers, "Accounting for high frequency transmission line loss effects 708 in HFSS," in *Proc. Ansoft User Workshop*, 2003 [Online]. Available: 709 http://www.ansoft.com 710

[30] Sonnet EM Software [Online]. Available: www.sonnetusa.com 711

[31] CST Microwave Studio [Online]. Available: www.cst.com 712

Eoin McGibney received the Ph.D. degree in elec- 713 tronic engineering from the Cork Institute of Tech- 714 nology, Bishopstown, Cork, Ireland, in 2009. 715

His research focused on the measurement and 716 modeling of IC packaging and materials for high 717 frequency applications. Since 2006, he has been a 718 Test Development Engineer with the Digital Video 719 Product Group, Analog Devices, Limerick, Ireland. 720 His current research interests include the field of 721 design for test for mixed signal ICs. 722

IEEE Proof

723 724 725 726 727 728 729 730 731 732 733 734 735

John Barrett is the Head of Academic Studies with the Nimbus Center for Embedded Systems Research, Cork Institute of Technology (CIT), Bishopstown, Cork, Ireland, and is the Group Director of the Center's Smart Systems Integration Research Group. He has been a Lecturer and Researcher with CIT since 1999, and was previously an Assistant Director of the Irish National Microelectronics Research Center (now Tyndall National Institute), Cork. His current research interests include packaging, miniaturization, and embedding of smart systems in materials, objects, and structures with particular emphasis on challenging and harsh application environments.

John Barton received the M.Eng.Sc. degree from University College Cork, Cork, Ireland, in 2006.

He joined the Interconnection and Packaging Group, National Microelectronics Research Center (now Tyndall National Institute), Cork, as a Research Engineer in 1993. Currently, he is with the Wireless Sensor Networks Team where his current research interests include ambient systems research, wearable computing, high density flexible interconnect, wireless sensor networks, and materials research for 3-D packaging. As PI on the Enterprise Ireland Funded D-Systems Project, he has been the leader of the development of the Tyndall Wireless Sensor Mote Platform. He has authored or co-authored over 90 peer-reviewed papers.

736 737 738 739 740 741 742 743 744 745 746 AQ:6 747 748 749

IEEE Proof

AUTHOR QUERIES

AUTHOR PLEASE ANSWER ALL QUERIES

750
751 AQ:1= Please provide affiliation lines and biographies of authors "Liam Floyd, Paul Tassie."
752 AQ:2= Please provide page range in Ref. [1].
753 AQ:3= Please provide vol. no. in Ref. [2].
754 AQ:4= Please provide month in Ref. [26].
755 AQ:5= Please update Ref. [28].
756 AQ:6= Please provide the expanded form of "PI."

757 END OF ALL QUERIES

IEEE Proof